Cell Insight 3 (2024) 100184

Contents lists available at ScienceDirect

Cell Insight

journal homepage: www.journals.elsevier.com/cell-insight

Research Article

Transcriptomic analysis of mouse TRAMP cell lines and tumors provide insights into shared pathways and therapeutic targets

Marxa L. Figueiredo [a,*], Sagar Utturkar [b], Shreya Kumar [a], Carlos Eduardo Fonseca-Alves [c,d]

[a] Department of Basic Medical Sciences, College of Veterinary Medicine, Purdue University, West Lafayette, IN, 47907, USA
[b] Purdue Institute for Cancer Research Computational Genomics, Purdue University, West Lafayette, IN, 47907, USA
[c] Institute of Health Sciences, Paulista University-UNIP, Bauru, 17048-290, Brazil
[d] School of Veterinary Medicine and Animal Science, São Paulo State University – UNESP, Botucatu, 18610160, Brazil

HIGHLIGHTS

- We conducted gene expression profile analyses in prostate cancer models to reveal distinct pathways.
- A novel gene signature was identified in aggressive TC2R tumors linked to poor prognosis.
- Altered TC2R tumor immune cell landscapes could be validated in a human bone metastatic prostate cancer scRNA-seq dataset.
- This model is relevant for testing preclinical therapeutics for prostate cancer.

GRAPHICAL ABSTRACT

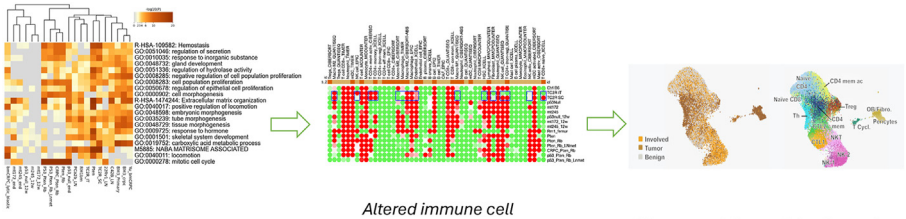

Gene expression profile analyses of TC2R tumors aligned with several datasets

Altered immune cell landscapes validated in a human single-cell RNA-seq from bone metastatic prostate cancer

Mouse model promising for testing preclinical therapeutics for prostate cancer

ARTICLE INFO

Keywords:
Prostate cancer
Mouse models
TRAMP transgenic model
RNA-Seq
Transcriptomic analysis
Immunocompetent models
Tumor progression

ABSTRACT

The present study focused on comparing the gene expression profiles of different mouse models of prostate cancer, focusing on the TRAMP transgenic model and its derived cell lines and extending the comparisons to relevant genetically engineered mouse models and human prostate cancer datasets. Employing RNA sequencing, we examined different levels of prostate cancer aggressiveness from the original TRAMP cells to the TRAMP-C2 (TC2) derived cell line and extending to the aggressive TC2-Ras (TC2R) cells and tumors. TC2R acquire the ability to grow in bone tissue upon implantation, unlike the parental TC2 cells. Analysis identified upregulated genes in cell cycle regulation, immune response, and mitotic processes in TRAMP compared to wild-type tissues. TC2 cells exhibited unique gene profiles enriched in ECM organization and tissue development pathways, while TC2R cells showed increased cytokine signaling and motility genes, with decreased ECM and immune response pathways. *In vivo* TC2R models demonstrated enhanced ECM organization and receptor tyrosine kinase signaling in tumors, notably enriching immune processes and collagen degradation pathways in intratibial tumors. Comparative analysis among mouse and human datasets showed overlaps, particularly in pathways relating to mitotic cycle regulation, ECM organization, and immune interactions. A gene signature identified in TC2R tumors correlated with aggressive tumor behavior and poor survival in human datasets. Further immune cell landscape analysis of TC2R tumors revealed altered T cell subsets and macrophages, confirmed in single-cell RNA-seq from human samples. TC2R models thus hold significant promise in helping advance preclinical therapeutics, potentially contributing to improved prostate cancer patient outcomes.

* Corresponding author. Department of Basic Medical Sciences, College of Veterinary Medicine, Purdue University, 625 Harrison St, LYNN 2177, West Lafayette, IN, 47904, USA.
E-mail address: mlfiguei@purdue.edu (M.L. Figueiredo).

https://doi.org/10.1016/j.cellin.2024.100184
Received 5 February 2024; Received in revised form 9 July 2024; Accepted 9 July 2024

1. Introduction

Prostate cancer is a complex and heterogeneous disease, and the development of reliable mouse models has significantly contributed to understanding its underlying molecular mechanisms. Among these models, the transgenic adenocarcinoma of the mouse prostate (TRAMP) model and its derived cell lines have been utilized as valuable tools for studying cancer progression and for identifying potential therapeutic targets (Kido et al., 2019). The TRAMP mouse model contains the minimal −426/+28 rat probasin promoter, which drives expression of the SV40 large T antigen (TAg) within the dorsolateral epithelium of the prostate (Greenberg et al., 1995). The SV40 TAg is a viral protein with potent oncogenic properties due to its binding to the tumor-suppressor gene products Rb (DeCaprio et al., 1988) and p53 (Lane & Crawford, 1979; Linzer & Levine, 1979). TAg expression induces the development of prostate tumors which resemble human prostate adenocarcinoma. Prostate tumors in these mice closely mimic some features of human prostate cancer, making them a valuable model for understanding the disease and testing potential therapeutic approaches.

The TRAMP-C2 (**TC2**) cell line (Foster et al., 1997), derived from a TRAMP prostate tumor, can grow *in vivo* following subcutaneous or intra-prostatically implantation. Despite being a mouse cell line, studying its transcriptome reveals shared biological pathways and dysregulated genes, shedding light on molecular mechanisms in common with human prostate cancer. TC2 has been utilized as a preclinical model for evaluating the effectiveness of therapeutic interventions (Chen et al., 2022; Dzojic et al., 2006; Lardizabal et al., 2018). However, one limitation is their inability to grow within bone following intratibial implantation. Therefore, we developed TC2-Ras (**TC2R**) as part of our research on bone metastatic and immune competent mouse models of prostate cancer (Umbaugh et al., 2018; Zolochevska et al., 2013). We initially examined different oncogenes for their ability to alter the tropism of TC2 for bone, and only Lv-Hras (moi = 2) could induce this phenotype, as compared to cells transduced with lentiviruses expressing other oncogenes. The introduction of an activated *H-Ras* oncogene resulted in significant changes in their characteristics compared to the original TC2 cells. TC2R cells exhibited more aggressive features, including faster growth *in vivo* (Umbaugh et al., 2018) and the ability to grow in bone when implanted intratibially (Zolochevska et al., 2013). This phenotype was of particular interest since bone metastasis is a significant complication of advanced prostate cancer. The development of the TC2R cell line and the bone implantation model has provided us with a valuable tool for testing new therapeutics for treating more aggressive prostate cancer phenotypes.

In the present study, we aimed to perform a comparative transcriptomic analysis of TRAMP-derived prostate cancer cell lines to elucidate conserved biological pathways and identify potential therapeutic targets relevant to human prostate cancer datasets. Additionally, we investigated gene expression changes in the TC2 and TC2R cell lines relative to the original TRAMP prostate, considering the influence of different tumor implantation sites - subcutaneous and intratibial. To achieve these objectives, we employed RNA-seq differential expression analysis and bioinformatics tools such as *Metascape* (Zhou et al., 2019), ShinyGO (Ge et al., 2020), and *Cytoscape* (Shannon et al., 2003), to identify pathways and biological processes influenced by the presence of the Ras variant, as well as processes underlying the bone growth capability of TC2R cells. We intially compared gene expression profiles of TC2R tumors with human prostate cancer datasets, including those associated with bone metastasis. We also examined the immune landscape of TC2R tumors relative to genetically modified mouse models (p53, Rb, Pten) and the common intratibial RM1 (Ras/Myc) model, validating the findings in a human single-cell RNAseq dataset from bone metastatic prostate cancer. The identification of overlapping differentially expressed genes, processes, and immune landscape between TC2R mouse models and human datasets further emphasize the relevance of these models for preclinical testing of agents with translational potential.

2. Materials and methods

Acquisition of RNAseq and scRNAseq datasets. RNAseq data was also compiled from various studies from other groups, summarized in Table S1, and utilized in a comparative manner with our datasets, all of which have been aligned as described below to enable their evaluation. RNA libraries were prepared for sequencing using standard Illumina protocols. Briefly, the RNAseq study describing TRAMP vs. wild-type (WT) prostate was published in (Wu et al., 2021), with RNA extracted using an AllPrep DNA/RNA kit (Qiagen, Germantown, MD) and deposited as GSE140310 (WT C57/BL6 prostate, 16 and 24 wks; TRAMP 16 and 24 wks). The study describing TRAMP-C2 (TC2) cells was published in (Lu et al., 2015) and total RNA isolated with RNeasy kit (Qiagen) and deposited as GSE75760. The other datasets include TRAMP-C2-Ras (TC2R) subcutaneous and intratibial tumors (Table S1). The single-cell RNA sequencing (scRNAseq) dataset was from human patient samples, including benign inflammation (Benign), involved bone marrow surrounding the tumor (Involved), and tumor isolates (Tumor) from bone metastatic castration-resistant prostate cancer (CRPC, GSE143791). This integrated scRNAseq dataset comprised samples from 9 metastatic CRPC patients and 7 benign inflamed bone marrow controls (Kfoury et al., 2021). In this study, comparisons were made between tumor samples and involved bone marrow (surrounding the tumor), with benign inflamed bone marrow serving as the control.

RNA isolation and qPCR. For the datasets generated from our group, we isolated total RNA and RNAseq performed with the samples as follows, with datasets deposited as listed in Table S1. For the TC2R cell line, first described in (Umbaugh et al., 2018), we isolated RNA from cell pellets using a RNAeasy kit (Qiagen) according to manufacturers' specifications. The study describing the TC2R cells was published in (Figueiredo Neto et al., 2020) and GSE248482. For tumor studies, post-euthanasia, collection was made in RNAlater (Invitrogen, Waltham, MA) and preserved for further RNA isolation and analysis. Briefly, tumors were preserved in RNAlater at 4 °C for up to 1 week to preserve RNA integrity. RNAlater was aspirated off tumor tissue, with tissues subsequently stored at −80 °C. Total RNA was isolated by adding 600 μL of RLT buffer and 10 μL of β-Mercaptoethanol to tumor sections, and homogenized with a PRO200 instrument (MidSci, ValleyPark, MO, United States) in three brief pulses of 10–15 s each at a mid-power. Lysates were then processed using the Qiagen RNAeasy kit (Qiagen) and eluted in 32 μL nuclease-free water (Ultrapure DNAse/RNAse-free distilled water, ThermoFisher, Waltham, MA).

Bioinformatics Analysis. Raw reads were trimmed using fastp (Chen et al., 2018) (version 0.23.2). Quality trimmed reads were aligned to the mouse (GRCm38) genome using the STAR aligner (Dobin et al., 2013) (version 2.7.10a). Reads aligned to each gene feature were quantified using featureCounts program (Liao et al., 2014) from Subread package (version 1.6.1). Differential expression (DE) analysis was performed using the edgeR (Robinson et al., 2010) method (version 3.40.2) and genes with False Discovery Rate (FDR) ≤ 0.05 and log2 (fold-change) $> |1|$ were denoted as significant. The immune landscape analyses used ImmCellAI (Miao et al., 2020) and TIMER2.0 (Li et al., 2020); clustering and figure preparation used Morpheus (https://software.broadinstitute.org/morpheus). Examination of the gene signature in human prostate tumors utilized GEPIA2 (Tang et al., 2019) and the Human Protein Atlas (proteinatlas.org, accessed June 15, 2024). Our analyses of the human scRNAseq dataset were performed using an open-source analysis toolkit (Trailmaker, https://www.parsebiosciences.com/data-analysis/), functionally annotating different subsets of T cell, Monocyte and B cell, and Cancer cell subsets by using scType and also differential gene expression to identify significant differences between similar subpopulations, based on the gene expression signatures described in detail in references (Hirz et al., 2023; Kfoury et al., 2021).

***Metascape, ShinyGO* Enrichment analyses and Cytoscape networks.** We utilized Metascape (Zhou et al., 2019), a web-based tool for gene annotation and functional enrichment analysis [accessed July 3,

2024], to gain insights into the biological processes and pathways associated with our gene expression data. Metascape integrates multiple databases and algorithms to provide comprehensive functional enrichment analysis, allowing us to explore the biological significance of our gene lists. To perform the functional enrichment analysis, we first uploaded our gene list to the Metascape (Zhou et al., 2019) website (https://metascape.org/). We specified the appropriate species and selected the desired gene annotation resources and pathway databases. Metascape yielded enrichment scores and p-values to identify significantly enriched gene ontology terms, biological processes, and pathways. Differentially expressed gene (DEG) lists were selected for Metascape analyses with a log2FC > 2 or -2 and $p < 0.01$. All annotations terms were selected, membership category included all functional sets, pathways, and structural complexes. For enrichment analysis (custom) settings, a minimum overlap of 3 and $p< 0.05$ were selected for pathways and processes, with the PPI enrichment combined (all) databases. To visualize and analyze the enriched terms and pathways, we employed Cytoscape version 3.9.1, an open-source software platform for network visualization and analysis (Shannon et al., 2003). This enabled us to explore the relationships between enriched terms, identify key hub genes, and gain an understanding of the functional interactions within our gene set.

For the *commonalities among TC2Ras tumors and various cell line or prostate cancer tumor datasets* (Fig. 7), we utilized Metascape with the top 500 DEGs upregulated in each sample for the comparison, except for bm1 and bm2 data, described as follows. The datasets utilized included: PCa2b_LN: human MDA-PCa2b bone metastatic prostate cancer DEGs relative to LNCaP (GSE110903); C42B_LN: human C4–2B bone metastatic prostate cancer DEGs relative to LNCaP (European Nucleotide Archive, PRJEB4877; ERS363579 and ERS363581 for LNCaP and C4–2 B RNAseq data); bm1: DEGs from the Table S1 published by Yu, 2020 et al. (Yu et al., 2020); bm2: DEGs from Table S2 published by Ihle et al., 2019 (Ihle et al., 2019); bm3: DEGs from human bone metastatic prostate cancer relative to normal prostate (GSE32269); 22Rv1_LN: DEGs from human CWR22Rv1 relative to LNCaP using GEO2R (GSE49287); TC2R_SC: DEGs from TC2-Ras subcutaneous tumors (GSE178142) relative to TC2Ras cells; TC2R_IT: DEGs from TC2-Ras intratibial tumors (GSE248482), relative to TC2Ras cells. P53 null and mutated tumors (GSE209532) (Mejía-Herná et al., 2022), Pten, Rb, and p53 tumors (GSE90891), and RM1 bone marrow tumor (femur; GSE147099).

3. Results

3.1. Tissues or cells selected represent various stages of TRAMP tumor development or phenotype

We selected tissues or cells representing a range of spectra of tumor formation or metastatic potential with basis on the TRAMP model (Fig. 1). These mice have the prostate-specific rat probasin promoter driving expression of the Simian Virus 40 large tumor T antigen (TAg), spontaneously develop progressive forms of prostate cancer from precancerous prostatic intraepithelial neoplasia, well-differentiated carcinoma, poorly differentiated adenocarcinoma of the prostate gland, and finally metastasis (Greenberg et al., 1995). TRAMP mice and subsequent cell lines were in the C57BL/6 background. We utilized data from in house RNA-seq or alignments with publicly available data as per the *Materials and Methods* to generate the comparisons described in the next sections, utilizing the TRAMP-C2 (TC2) and TRAMP-C2-Ras (TC2R) cell lines, as well as tumor models using TC2R *in vivo*, subcutaneously, or intratibially.

3.2. TRAMP up- and down-regulated genes relative to wild-type (WT) prostate

For the differentially expressed genes (DEGs) *upregulated in TRAMP* prostates (16–24 weeks) relative to Normal (wild-type or WT) prostate, (Fig. 2a), the analysis revealed enriched Reactome processes related to *Cell cycle,* in particular the *DNA synthesis and M phases*, *Mitotic prometaphases*, *Resolution of sister chromatid cohesion*, *Amplification of the signal from kinetochores*, *and Rho GTPases activation of Formins.* The enrichment analysis with GO biological processes indicated upregulation of several *processes relating to Immune response*, *Cell cycle*, *Interactions with organisms* or *responses to external stimuli*, and the *Mitotic cell cycle* and *chromosome*

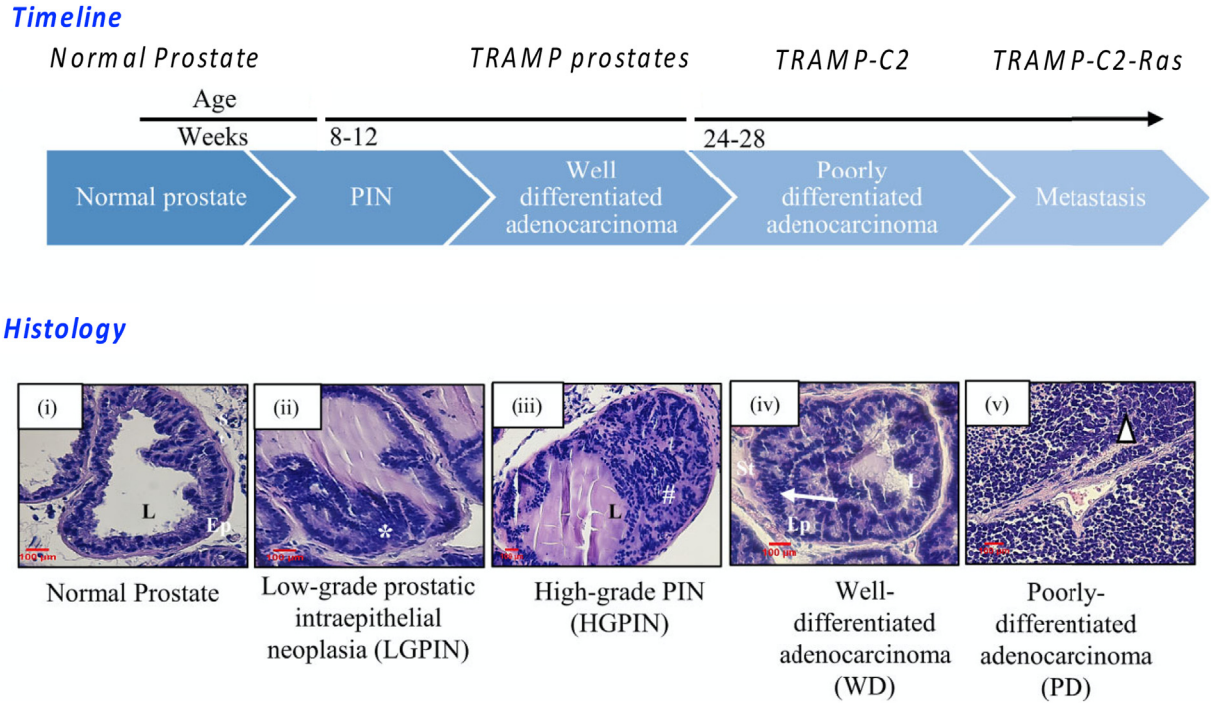

Fig. 1. Graphical summary of the timeline and tissue types during the TRAMP prostate tumor progression. This figure illustrates how the cell lines used in this study can model aspects of advanced tumor growth *in vivo*. Modified from *Ganguly K et al. (2022). Front. Immunol. Vol 13*, https://doi.org/10.3389/fimmu.2022.930449, licensed under Creative Commons CC BY 4.0.

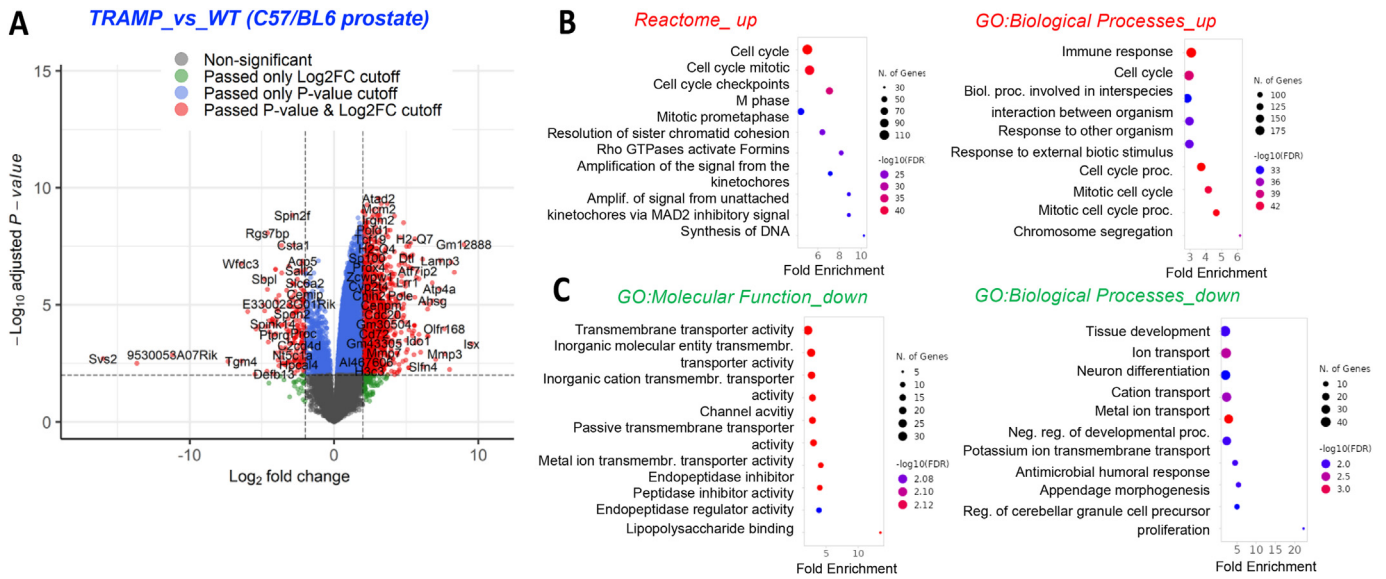

Fig. 2. Comparison of the TRAMP vs. WT (Normal prostate) transcriptomes. (A) DEGs up and downregulated in TRAMP vs. WT prostate (C57/BL6); (B) Pathways and processes enriched in the upregulated DEGs; *Right plot: GO:Biological Processes; Left plot: Reactome.* (C) Pathways and processes enriched in the downregulated DEGs; *Right plot: GO:Biological Processes; Left plot: Reactome.* The genes were filtered based on criteria fold change >2.0 and $p < 0.05$ (1009 up) and with FC < −1.5 and $p < 0.05$ (346 down) to obtain gene lists inputted into ShinyGO 0.77 for analysis.

segregation (Fig. 2b).

For the *DEGs downregulated in in TC2* relative to the TRAMP prostate (Fig. 2c), the analysis showed no enriched Reactome processes, yet Molecular Functions enriched included several *transmembrane transport* processes and *channel activities*, as well as *endopeptidase activity, peptidase activity,* and *Lipopolysaccharide binding*. The enrichment analyses with GO biological processes indicated downregulation in processes relating to *Tissue development, Neuron differentiation*, *Transport of cations*, *ions*, *potassium and metal ions*, *Negative regulation of developmental processes*, *Appendage morphogenesis*, and *Antimicrobial humoral response*, among others.

3.3. TRAMP-C2 up- and down-regulated DEGs relative to TRAMP

For the DEGs *upregulated in TC2* relative to the TRAMP prostate (Fig. 3a), the analysis revealed enriched Reactome processes related to *ECM organization*, *Collagen formation/biosynthesis*, *Trimerization, and Assembly of fibrils*, *Degradation of the ECM and Glycosaminoglycan metabolism*, *O-glycosylation of TSR domain containing proteins.* The enrichment analysis with GO biological processes indicated upregulation of several *Tissue development* and blood *vasculature development* functions, as well as ECM organization and organization of extracellular structures (Fig. 3b).

For the *DEGs downregulated in TC2* relative to the TRAMP prostate (Fig. 3c), the analysis showed enriched Reactome processes related to *Metabolism of lipids (fatty acid and phospholipid), Transport of small molecules, SLC-mediated transmembrane transport* and *Transport of inorganic cations/anions* as well as *Amino acids and oligopeptides, Trans-Golgi network vesicle budding*, and *Formation of cornified envelope*, the enrichment analyses with GO biological processes indicated downregulation in processes relating to *nitrogen compound*, *transmembrane*, *ion transport*, *Lipid and small*

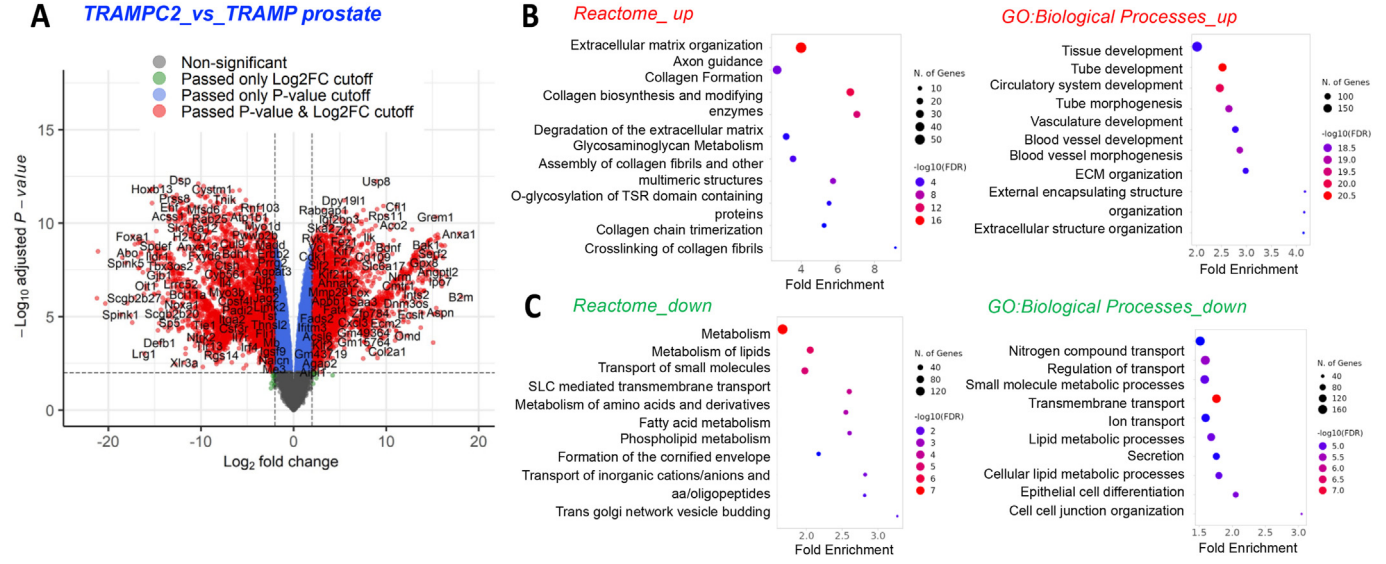

Fig. 3. Comparison of the TRAMP-C2 vs. TRAMP transcriptomes. (A) DEGs up and downregulated in TRAMP vs WT prostate (C57/BL6); (B) Pathways and processes enriched in the upregulated DEGs; *Right plot: GO:Biological Processes; Left plot: Reactome.* (C) Pathways and processes enriched in the downregulated DEGs; *Right plot: GO:Biological Processes; Left plot: Reactome.* The genes were filtered based on criteria fold change >2.0 and $p < 0.00001$ (1210 up) and with FC < −2.0 and $p < 0.00001$ (1352 down) to obtain gene lists inputted into ShinyGO 0.77 for analysis.

molecule metabolism, *Secretion*, *Cell-cell junction organization*, and *Epithelial cell differentiation.*

3.4. TRAMP-C2-ras up- and down-regulated DEGs relative to TRAMP-C2

For the DEGs *upregulated in TRAMP-C2-Ras (TC2R)* relative to TC2 (Fig. 4a), the analysis revealed enriched Reactome processes related to *Cytokine and interleukin signaling*, *MAPK family* (and *negative regulation of MAPK signaling*) and *FLT3 signaling.* The *Cargo recognition for Clathrin-mediated endocytosis*, *Fatty acyl-CoA biosynthesis*, and *RAF-independent MAPK1/3 activation* were also highly enriched in the TC2R upregulated DEG list. The enrichment analysis with GO biological processes indicated upregulation of several *Cell motility* and *Migration* functions, as well as *Negative regulation of signal transduction*, *Cellular responses to cytokines*, and *Cell-cell adhesion via plasma membrane molecules* (Fig. 4b).

For the *DEGs downregulated in TC2R* relative to TC2 (Fig. 4c), the analysis showed enriched Reactome processes related to ECM organization and degradation, in particular, collagen formation and degradation, ECM proteoglycans, and MET activated PTK2 signaling. The enrichment analyses with GO biological processes indicated downregulation in *defense response* mechanisms and *interaction with other organisms*, *innate immune response*, *ECM organization*, and *Extracellular structure organization.*

3.5. TC2R subcutaneous tumors and TC2R comparison of transcriptomes

For the differentially expressed genes (DEGs) *upregulated in TC2R SC tumors* relative to the TC2R cell line (Fig. 5a), the analysis revealed enriched Reactome processes related to *Metabolism, Signaling by receptor tyrosine kinases, ECM organization and ECM proteoglycans,* and several *Translation* related processes, as well as *Respiratory electron transport.* The enrichment analysis with GO biological processes indicated the upregulation of several *locomotion*, *cell motility*, and *migration* functions, as well as *vasculature development* (Fig. 5b).

For the *DEGs downregulated in TC2R SC tumors* relative to the cell line (Fig. 5c), the analysis showed enriched Reactome processes related to protein *metabolism* and *post-translational modification*, as well as several *transcription* related pathways, *RNA processing*, and *pathways regulating TP53 activity*. The enrichment analyses with GO biological processes indicated downregulation in *cell cycle* (including *negative regulation of the cell cycle*) and *cell protein localization*, including *protein localization to organelles,* and processes related to *embryonic development.*

3.6. TC2R intratibial tumors and TC2R comparison of transcriptomes

For the DEGs *upregulated in TC2R intratibial (IT) tumors* relative to the cell line (Fig. 6a), the analysis revealed enriched Reactome processes related to *Immune System, neutrophil degranulation*, *BCM organization, signaling by RTKs*, *collagen degradation and ECM proteoglycans*, *platelet activation signaling and aggregation, non-integrin membrane-ECM interactions*, and *MET activates PDK2 signaling.* The enrichment analysis with GO biological processes indicated upregulation of several *locomotion*, *cell motility*, and *migration* functions, as well as *negative regulation of multicellular organismal processes* (Fig. 6b).

For the *DEGs downregulated in TC2R IT tumors* relative to the cell line (Fig. 6c), the analysis showed enriched Reactome processes related to *Transcription.* The enrichment analyses with GO biological processes indicated downregulation in processes relating to *the positive regulation of biosynthesis*, *cell migration*, and *response to cytokines*, and the negative regulation of *macromolecule biosynthesis*, *cell communication*, and *intracellular signal transduction.*

3.7. Connections between TC2R tumors relative to other datasets from mouse and human prostate cancer

A Metascape analysis indicated a high level of commonality between upregulated TC2R tumor DEGs and those from a variety of cell line, mouse models, or human prostate cancer datasets, pointing to a high relevance of the TC2R models to prostate cancer. The top-level gene ontology (GO) *biological processes* showing enrichment in the samples assayed align with the underlying cellular activities and mechanisms relevant to prostate cancer. These processes encompassed a wide range of functions, including those highly significant (the lowest -log 10(P) values): *regulation of cell proliferation*, *tube and tissue morphogenesis*, *response to hormone*, *skeletal system development*, *NABA matrisome associated*, *locomotion*, *mitotic cell cycle*, and *response to inorganic substance.* These clustered with RM1_bm, PCa2b, p53_null, and Pten models most closely, but were also similar to 22Rv1, C42–B, and three bone-metastatic castration resistant (bmCRPC) or primary prostate tumor human datasets (Fig. 7a). A transcription factor analysis by Metascape (TTRUST) predicting regulators upstream of the observed gene expression changes revealed the most similarity among TC2R models and p53_null, CWR_22Rv1, and a dataset from human bmCRPC (Fig. 7b). The genes up- or downregulated in the datasets were determined be enriched in regulatory elements for binding RelA, NfKB 1, Jun/JunD, STAT1/STAT3, SP1,

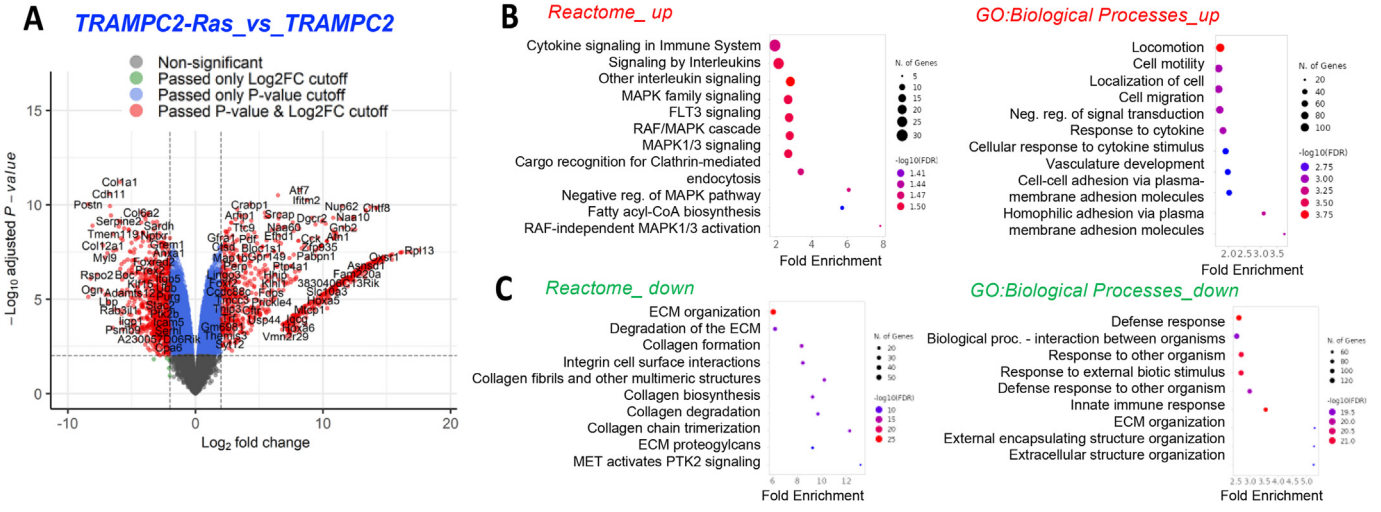

Fig. 4. Comparison of the TC2R vs. TC2 transcriptomes. (A) DEGs up and downregulated in TC2R vs. TC2; (B) Pathways and processes enriched in the upregulated DEGs; *Right plot: GO:Biological Processes; Left plot: Reactome.* (C) Pathways and processes enriched in the downregulated DEGs; *Right plot: GO:Biological Processes; Left plot: Reactome.* The genes were filtered based on criteria fold change >2.0 and $p < 0.05$ (773 up) and with FC < −2.0 and $p < 0.05$ (789 down) to obtain gene lists inputted into ShinyGO 0.77 for analysis.

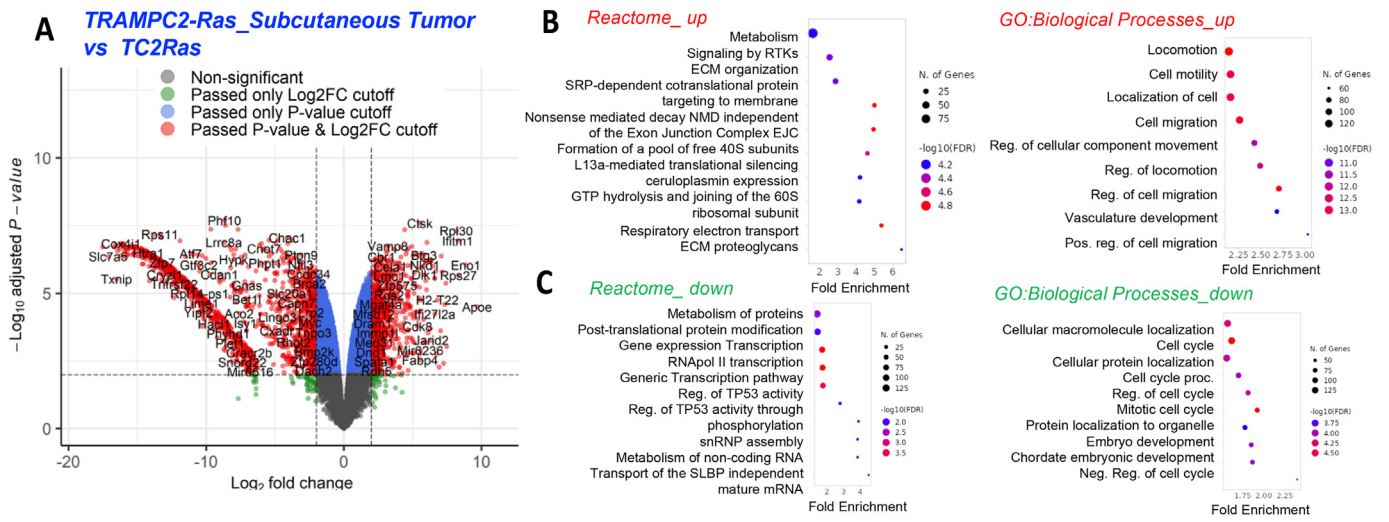

Fig. 5. TC2R Subcutaneous tumors vs. TC2R transcriptomes. A) DEGs up and downregulated in TC2R vs. TC2; (B) Pathways and processes enriched in the upregulated DEGs; *Right plot: GO:Biological Processes; Left plot: Reactome.* (C) Pathways and processes enriched in the downregulated DEGs; *Right plot: GO:Biological Processes; Left plot: Reactome.* The genes were filtered based on criteria fold change >2.0 and $p < 0.05$ (848 up) and with FC < −2.0 and $p < 0.05$ (1342 down) to obtain gene lists inputted into ShinyGO 0.77 for analysis.

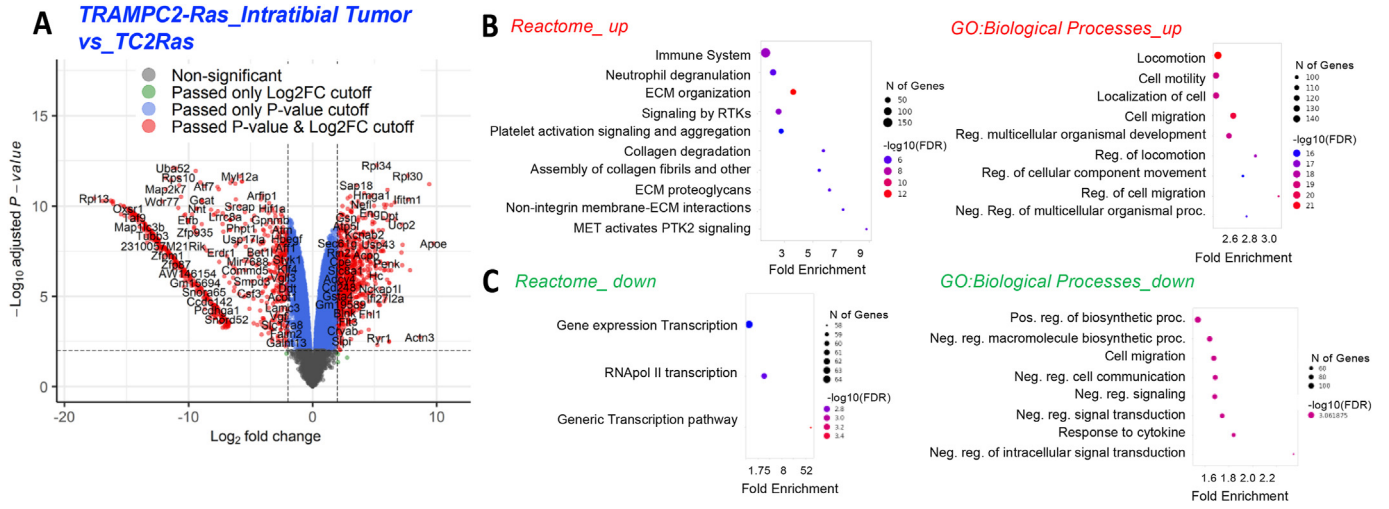

Fig. 6. TC2R Intratibial Tumor vs. TC2R transcriptomes. A) DEGs up and downregulated in TC2R vs. TC2; (B) Pathways and processes enriched in the upregulated DEGs; *Right plot: GO:Biological Processes; Left plot: Reactome.* (C) Pathways and processes enriched in the downregulated DEGs; *Right plot: GO:Biological Processes; Left plot: Reactome.* The genes were filtered based on criteria fold change >1.5 and $p < 0.05$ (1204 up) and with FC < −1.5 and $p < 0.05$ (923 down) to obtain gene lists inputted into ShinyGO 0.77 for analysis.

E2F1, TP53, HDAC1, and HIF1A.

The data obtained from *Metascape* using the Protein-protein Interaction Enrichment Analysis identified networks enriched among datasets which included TC2R. These findings suggested molecular mechanisms and pathways that contribute to prostate cancer aggressiveness in both mouse models and human samples, providing insights for further investigation and potential therapeutic targeting in prostate cancer. The genes in the network with connectivity between TC2R IT tumors and other models (mouse and/or human) formed a 12 gene signature: PRC1, BIRC5, KIFC1, CDKN2A, MMP10, MMP3, TIMP1, ASPN, NPTX1, FOSL1, HMGA2, FOXA2 (Fig. 8). These belonged to the key pathways *mitotic cell cycle*, *ECM organization, integrin1-syndecan* and *NABA core matrisome*, as well as roles in *cell junction organization*, *cell cycle and senescence*, and *hormone regulation*.

We further validated the TC2R IT 12-gene signature for its relevance to prostate cancer aggressiveness. We found that at least 9 of the proteins encoded by these genes were upregulated relative to normal tissues in human prostate cancer, either glandular or stromal areas (Fig. 9a). Also, this signature was significantly upregulated in human tumors relative to normal prostate tissue, particularly using unsupervised clustering of The Cancer Genome Atlas (TCGA) data in GEPIA2, which identifies molecular classes of human prostatic adenocarcinoma (PRAD) as 'iClusters'. The signature was significantly upregulated in subsets 'iClusters' 2 and 3 (Abeshouse et al., 2015; Shen et al., 2009) (Fig. 9b). Interestingly, upregulation of this gene signature in tumors correlated significantly with reduced survival in the PRAD dataset (Fig. 9c). These findings suggest that these targets may be relevant for examining therapies for prostate cancer using the TC2R intratibially generated model of bone metastases.

We also sought to better understand the immune landscape of TC2R tumors, starting with a comparison across genetically modified mouse models relevant to TC2R, particularly those with p53 and/or Rb modifications (Fig. 10). The results indicated similarities with several of the mouse models evaluated, detecting increases in NK cells in TC2R IT

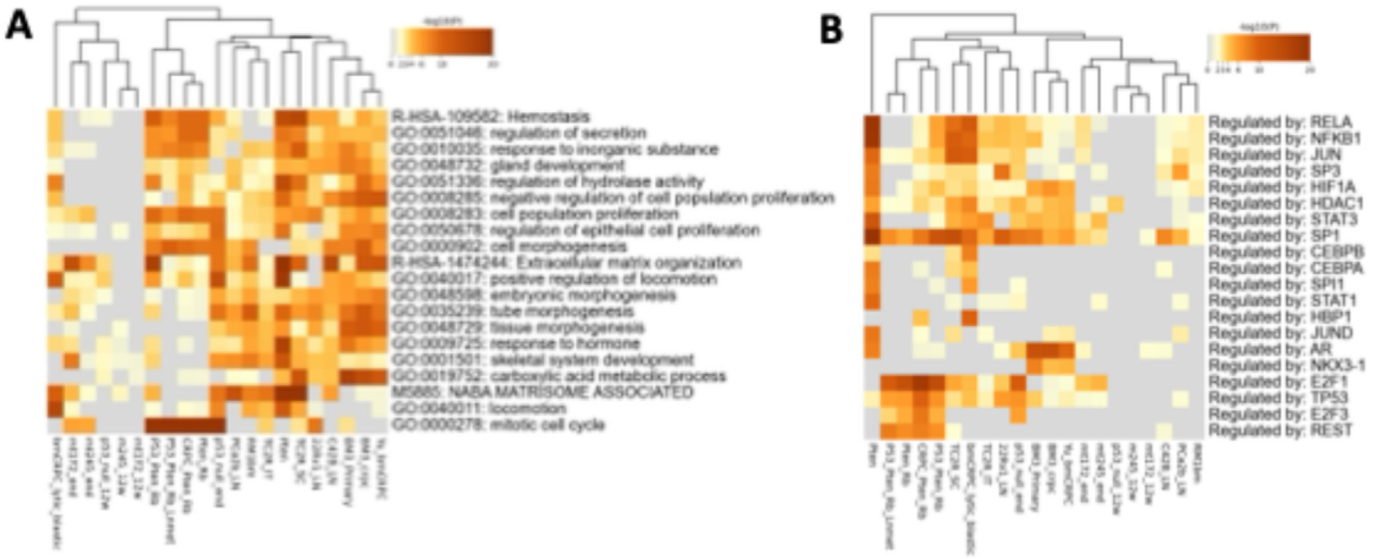

Fig. 7. Commonalities among TC2Ras tumors and various cell line or prostate cancer tumor datasets. (A) Common pathways between TC2Ras tumors (IT: intratibial, SC: subcutaneous) and several human and mouse models of prostate cancer ($p < 0.05$). The top 500 DEGs upregulated in each sample were used in the comparison, except where noted below. (B) TTRUST transcription factor analysis showing commonalities among human and mouse prostate cancer datasets. *Groups:* ***RM1_bm****: mouse prostate cancer implanted intratibially,* ***PCa2b_LN:*** *human MDA-PCa2b bone metastatic prostate cancer DEGs relative to LNCaP,* ***C42B_LN:*** *human C4–2B bone metastatic prostate cancer DEGs relative to LNCaP;* ***bm1:*** *human bone metastatic prostate cancer DEGs from Yu et al., 2020,* ***bm2:*** *human bone metastatic prostate cancer DEGs from Ihle et al., 2019;* ***bm3****: human bone metastatic prostate cancer DEGs relative to normal prostate,* ***22Rv1_LN:*** *DEGs from human CWR22Rv1 relative to LNCaP; p53 null or mutated mouse models (mt172 or m245 at 12 weeks or endpoint); Pten null mouse models including tissues from Pten crossed with p53 null or also Rb null, prostate cancer, or Lymph node metastases tissues.* ***TC2R_SC:*** *DEGs from TC2-Ras subcutaneous tumors relative to TC2Ras cells;* ***TC2R_IT:*** *DEGs from TC2-Ras intratibial tumors relative to TC2Ras cells. Accession numbers listed in the Materials and Methods.*

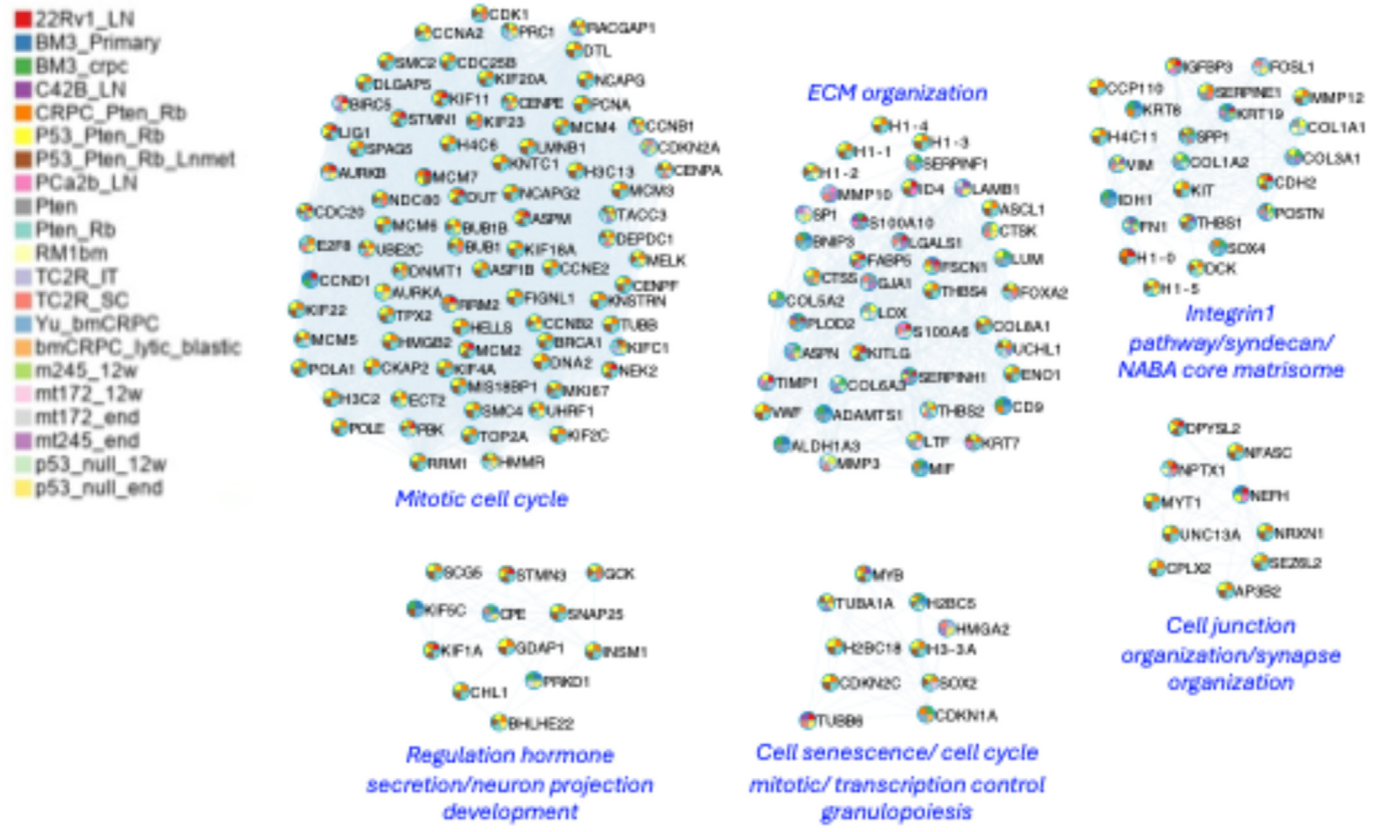

Fig. 8. Key interaction networks shared between TC2R tumors and other relevant prostate cancer-related datasets, including genetically modified mouse models (p53, Pten, Rb), a common intratibial implantation model (RM1_bm), and human advanced prostate cancer (castration resistant, CRPC or bone-metastatic (bm) CRPC) datasets.

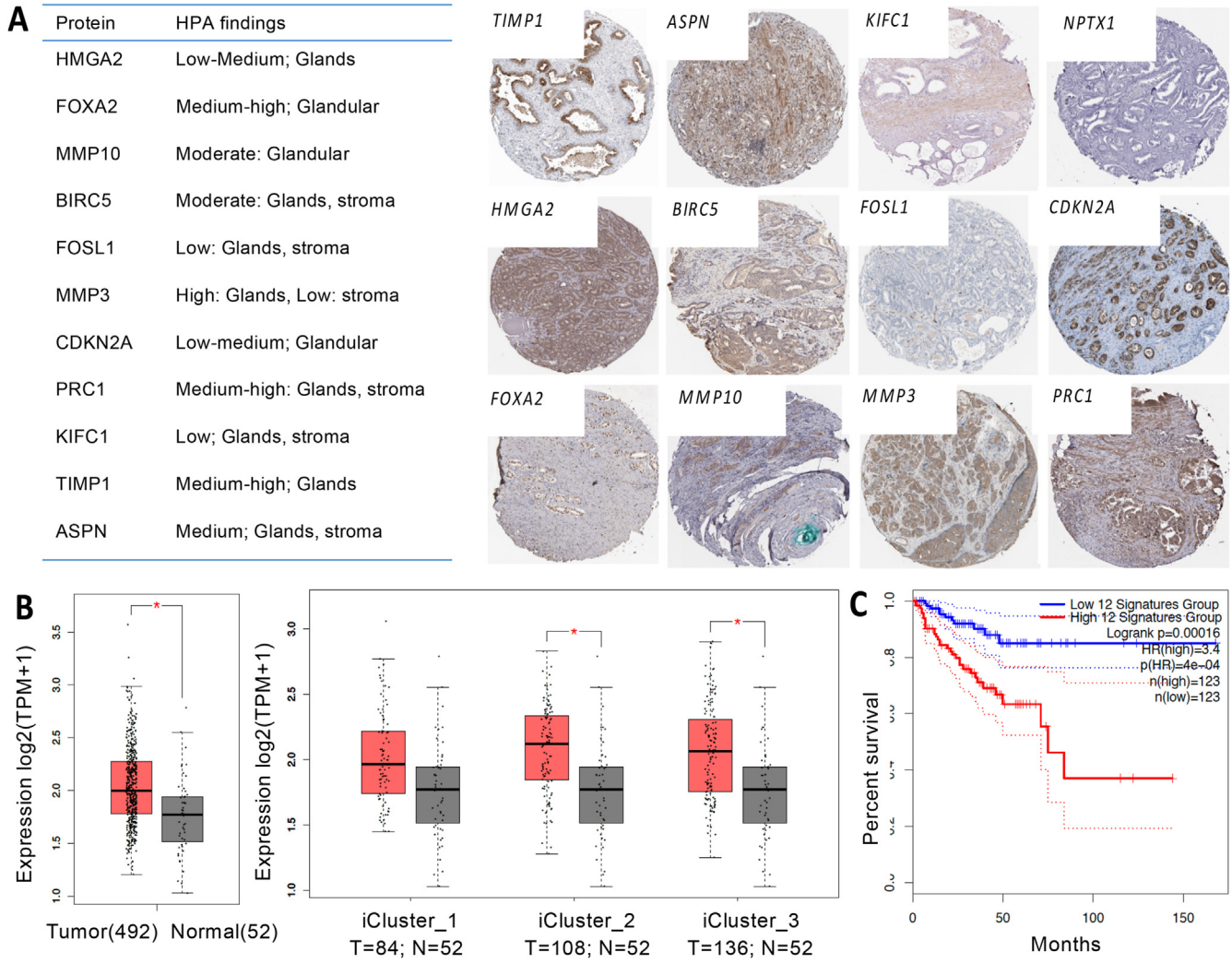

Fig. 9. Validation of the gene signature identified in TC2R intratibial tumors that overlaps with mouse and human datasets. (A) Protein detection for genes overlapping with the TC2R IT tumor dataset using the Human Protein Atlas. (B) Relevance to the human prostatic adenocarcinoma (PRAD) TCGA dataset, showing significant correlation with reduced disease-free survival ($p < 0.0002$) when the 12-gene signature is highly expressed, confirming its association with aggressive tumor behavior.

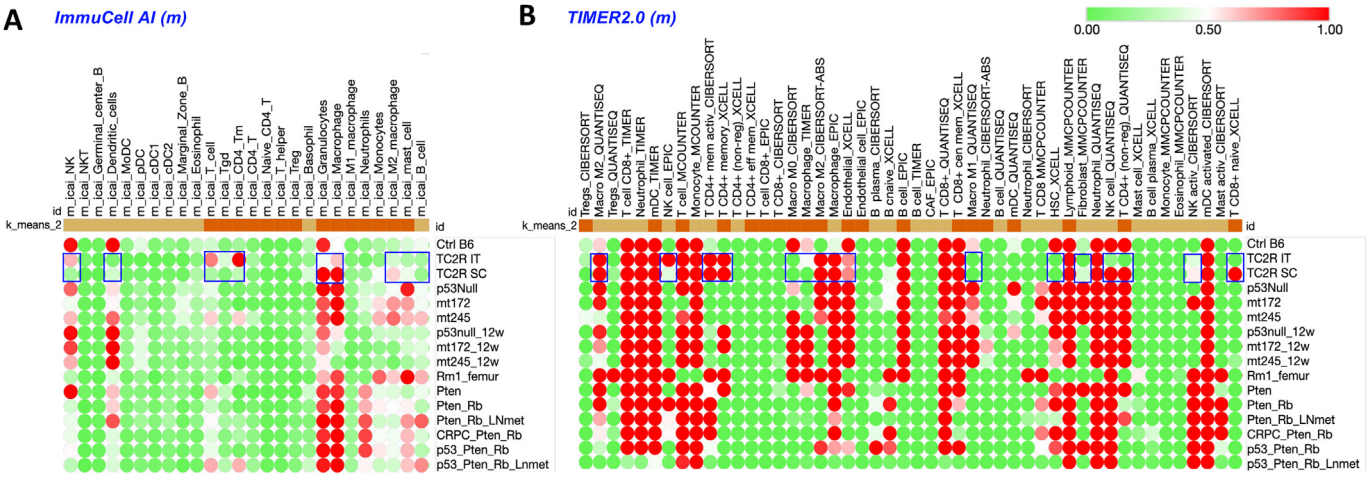

Fig. 10. RNAseq-based immune cell landscape in various relevant mouse models for comparison with TC2R tumors. The cells upregulated relative to control C57/BL6 prostate are indicated by red color, while downregulated cell types are indicated in green. (A) used the ImmuCellAI mouse deconvolution algorithm (Miao et al., 2020), and (B) utilized several algorithms available through TIMER2.0 (Li et al., 2020). Blue boxes highlight the key changes in immune cells with TC2R tumors. Analysis used K-means clustering by Morpheus (https://software.broadinstitute.org/morpheus).

tumors by ImmuCellAI, yet at low levels in an activated state (by TIMER2.0). Also, both activated and inactive CD4 T memory cells (Tmem/Tm) were detected, along with elevated M2 Macrophages, and reduced levels of M1 macrophages. In the SC model of TC2R, similar changes were detected, with indications of higher levels of granulocytes, naïve B cells, fibroblasts, NK cells, and CD8-naïve cells relative to the IT model. Fewer hematopoietic stem cells (HSCs) were detected in both models relative to control prostate tissue.

Finally, we aimed to validate the finding from our bulk RNAseq analysis of the mouse immune landscape using a human single-cell RNAseq dataset, focusing on bone-metastatic prostate cancer. As shown in Fig. 11, this dataset indicated alignment of several cell types and subtypes with the mouse findings. For example, the CD4 Tmem, Treg, and M2 macrophage populations overlapped with the mouse model findings. Also, since this was a single-cell RNAseq dataset, it enabled us to further refine the localization and characterization of dysfunctional T cell and monocytic lineages within these tumors. Populations enriched in the human tumors relative to surrounding bone marrow (involved) included T helper (Th), T lineage cycling/progenitors, osteoblasts/fibroblasts, and pericytes (Fig. 11a). Conversely, populations such as NK and NKT cells were present in the involved bone marrow but excluded from tumors. Two cytotoxic T cell populations described by reference (Kfoury et al., 2021) were idenitifed in tumors, including a more cytotoxic (CTL1), but also a dysfunctional CTL2 population. CD4 memory cells were also detected within the tumor fraction. In the monocytic subset (Fig. 11b), cell types present within tumors included inflammatory monocytes (TIMo), M1 macrophages, M2 macrophages, MDSC-like populations, some myeloid DCs, and B-naïve cells. Additionally, neutrophils, progenitor cells, mast cells, and osteoclasts were isolated alongside the tumor fraction.

Furthermore, we assessed the expression levels of the 12 gene-signature identified in Fig. 8 within TC2R IT tumors relative to other mouse and human prostate cancer datasets using the scRNAseq dataset from bone metastatic prostate cancer patients. We determined that several of the signature genes were expressed in specific cell clusters relating to progenitors/T cycling (KIFC1, CDKN2A, PRC1, BIRC5), as well as in osteoblasts/fibroblasts and activated CD4 memory T cells (TIMP1, ASPN) (Fig. 12a). In the monocytic-focused subset, TIMP1 was detectable across most cell types, with progenitors and mast cells expressing PRC1 and BIRC5, and a granulocytic-like MDSC cluster expressing BIRC5. FOSL1 was detected in several clusters, whereas MMP3 and MMP10 were not detected in any of these subsets (Fig. 12b). Within the cancer cell subset, three tumors were examined representing the bone metastases dataset. All three tumors showed relatively high levels of TIMP1 expression, whereas a couple of tumors expressed FOSL1, BIRC5, and one tumor each showed expression of KIFC1 or HMGA2 (Fig. 12c).

In conclusion, our analyses of networks, transcription factors, and enriched biological processes indicated significant similarity between the mouse models and the human prostate cancer cell lines or tumors examined. This suggests that the TC2R mouse models can capture key molecular features and regulatory networks that are relevant to the human disease. These models can potentially facilitate the translation of novel therapeutic strategies from preclinical to clinical settings, potentially paving the way for targeted interventions and personalized treatments that can benefit prostate cancer patients.

4. Discussion

Our study compared gene expression in different mouse models of

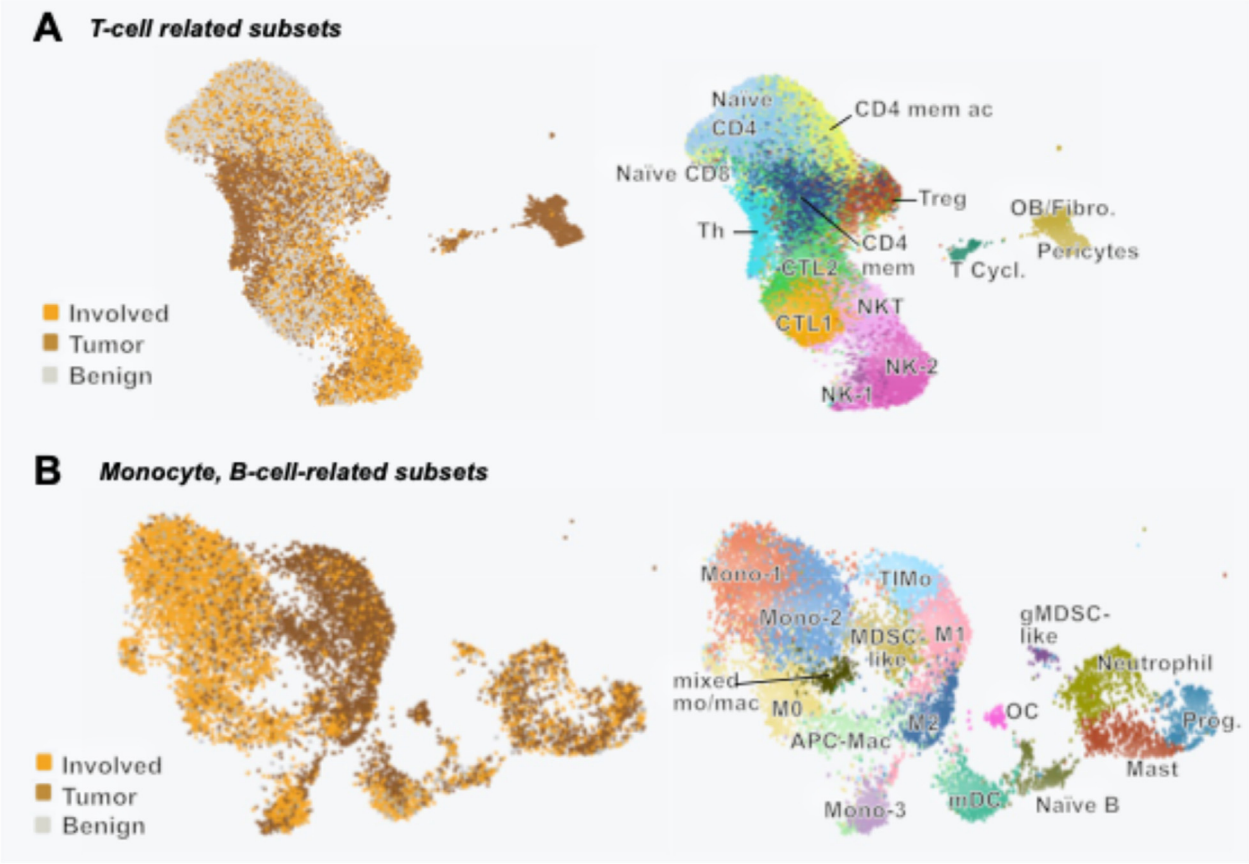

Fig. 11. Validation of the immune cell landscape using single-cell RNAseq data from bone metastatic prostate cancer patient samples. (A) T-cell subsets from 'involved' vertebral bone marrow surrounding the tumor, the bone-metastatic 'tumor' from each of the same patients, and controls from 'benign' inflammation samples (hip replacement patients) (B) Monocyte and B-cell related subsets within the same dataset as A. Annotations are described in *Materials and Methods* for GSE143791.

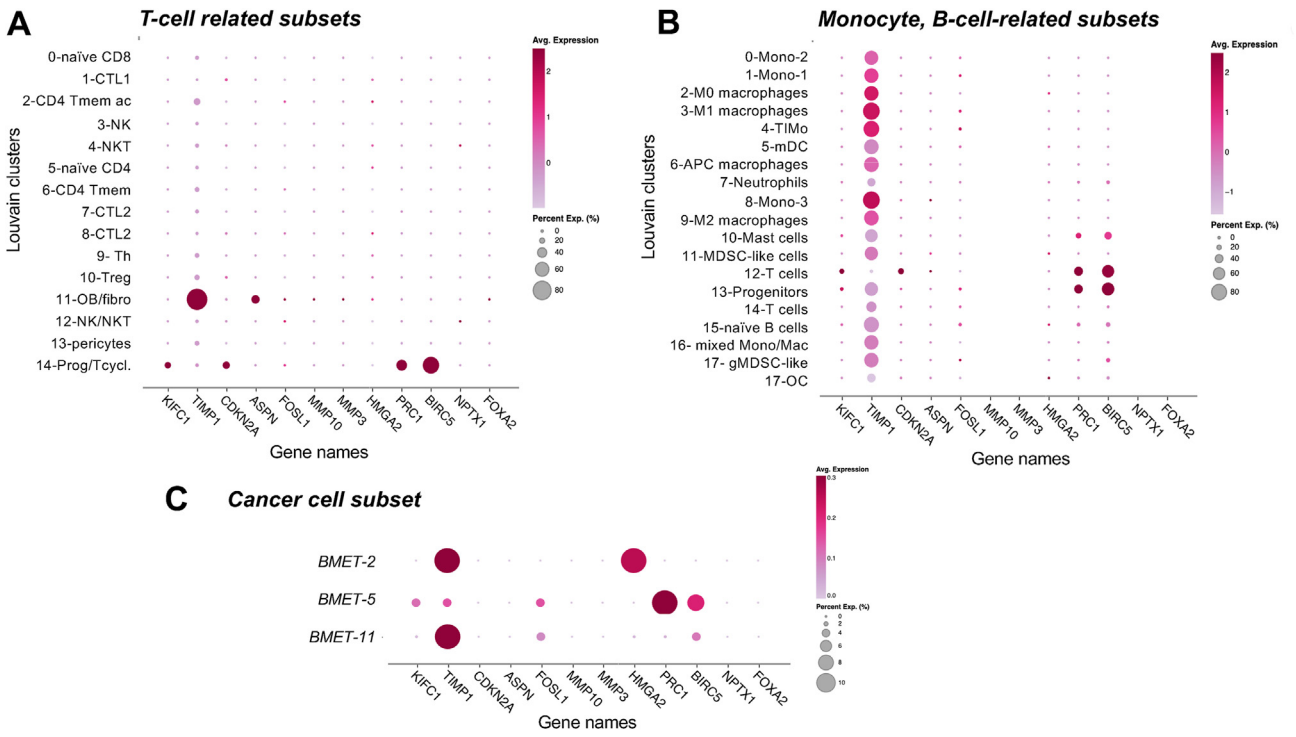

Fig. 12. Dot plots delineating the expression of the 12-gene signature shared by TC2R IT tumors and mouse and human prostate cancer models in a human scRNAseq dataset. (A), *T cell related subsets*; (B) *Monocyte and B cell related subsets*, and (C) *Cancer cell subset* from tumors of bone metastatic castration-resistant prostate cancer (GSE143791).

prostate cancer, specifically TRAMP transgenic models and derived cell lines. Using RNA sequencing (RNAseq), we examined the gene expression changes underlying the aggressiveness and ability to grow in bone of TC2R cells relative to less aggressive cells and models. For example, from the TRAMP prostate comparison to wild type, we observed significant molecular changes relating to the development of prostate cancer. Upregulated genes in TRAMP prostates were enriched in processes relating to cell cycle regulation, DNA synthesis, mitosis, and chromosome cohesion. These genes also were implicated in processes such as kinetochore signaling and Rho GTPase activation, suggesting enhanced cell proliferation. Additionally, upregulated genes were involved in immune responses, potentially reflecting tumor-immune interactions. Conversely, downregulated genes in TC2 relative to TRAMP were linked to transport, binding activities, developmental processes, ion transport, metabolism, and immune responses, indicating a shift towards a more aggressive and less differentiated state in TC2 prostate cells. The next comparison identified significant molecular distinctions between TRAMP and TC2. TC2 cells exhibited upregulated genes associated with ECM organization, collagen formation, fibril assembly, ECM degradation, glycosaminoglycan metabolism, and O-glycosylation of TSR domain proteins, suggesting alterations in the tumor microenvironment. Biological processes analysis indicated upregulation in genes enriched in processes including tissue structure and vascularization. Conversely, downregulated genes in TC2 cells were linked to lipid metabolism, small molecule transport, Trans-Golgi network vesicle budding, nitrogen compound transport, lipid metabolism, secretion, and cell-cell junction organization, indicating alterations in cellular processes, metabolism, and communication during prostate cancer progression. These findings confirmed that TC2 cells, known for hormone resistance, are valuable for studying therapy resistance, tumor progression, and metastasis mechanisms in prostate cancer.

Analysis of TC2R versus TC2 transcriptomes revealed important insights into molecular processes and pathways underlying the ability of TC2R to *(i)* grow faster than the parental TC2 line (Umbaugh et al., 2018) and *(ii)* to have gained the ability to grow within the bone microenvironment (Zolochevska et al., 2013) upon intratibial implantation, both indicating the transition to a more aggressive prostate cancer phenotype. Upregulated DEGs included cytokine and interleukin signaling, MAPK family signaling (activation and negative regulation), FLT3 signaling, endocytosis, fatty acyl-CoA biosynthesis, and MAPK1/3 activation independent of RAF, suggesting heightened cell signaling and tumor aggressiveness. Biological processes analysis indicated upregulation in cell motility, migration, locomotion, and negative regulation of signal transduction and immune responses, potentially enhancing cell movement and immune evasion in TC2R. Downregulated DEGs in TC2R involved ECM organization and degradation, collagen formation, ECM proteoglycans, defense responses, innate immune responses, and extracellular structure organization, indicating potential immune defense loss and ECM alterations in TC2R cells relative to TC2. These findings provided insights into the molecular changes driving the more aggressive phenotype observed in TC2R cells.

In the comparison of *TC2R subcutaneous* (SC) tumors to the TC2R cell line, upregulated DEGs were associated with processes related to metabolism, receptor tyrosine kinase signaling, ECM organization, translation, and respiratory electron transport. These tumors also exhibited upregulation in functions associated with cell motility, migration, and vasculature development, suggesting an active tumor microenvironment. Downregulated DEGs were enriched in processes including protein metabolism, transcription, RNA processing, and pathways regulating p53 activity, indicating potential alterations in cell cycle regulation and protein processing. In the comparison of *TC2R intratibial* (IT) tumors to the TC2R cell line, upregulated DEGs were enriched in immune-related processes, neutrophil degranulation, receptor tyrosine kinase signaling, collagen degradation, platelet activation, and ECM interactions. These tumors also showed upregulation in cell motility and migration functions, along with negative regulation of multicellular organismal processes. Downregulated DEGs were primarily enriched in transcription-related processes and showed reductions in biosynthesis, cell migration, response to cytokines, and the regulation of macromolecule

biosynthesis, cell communication, and intracellular signal transduction. These findings highlighted distinct molecular signatures in the two tumor types, with SC tumors displaying metabolic and protein processing alterations, and IT tumors exhibiting immune-related and ECM-related changes. These differences likely reflect the unique microenvironments and growth patterns of the tumors, suggesting that these two implantation sites potentially can be used to test therapeutics against different therapeutic targets or processes.

Integration of the *TC2R tumor* data with *human datasets* indicated molecular similarities with human prostate cancer, suggesting the relevance of these mouse models for therapeutic testing. Upregulated genes in TC2R tumors that clustered with other models showed enrichment in processes related to *regulation of cell proliferation, tube and tissue morphogenesis, response to hormone, skeletal system development, NABA matrisome associated, locomotion, mitotic cell cycle, and response to inorganic substance*. These processes clustered most closely with the RM1 bone implantation model, the PCa2b cell line, which causes osteoblastic lesions in bone, and the p53-null and Pten mouse models. TC2R IT tumors shared similar processes with the castration-resistant human line CWR22Rv1, the LNCaP subline C42–B, able to form osteoblastic lesions in bone upon implantation, as well as with three human bmCRPC or primary prostate tumor datasets. Dysregulation of these processes is known to contribute to prostate cancer development and progression. A transcription factor analysis identified regulators upstream of the DEGs, revealing the most similarity among TC2R models and p53-null, CWR22Rv1, and a dataset from human bmCRPC. The regulation by transcription factors RelA, NFκB1, Jun/JunD, STAT1/STAT3, SP1, E2F1, TP53, HDAC1, and HIF1A was implicated in driving the observed gene expression changes.

The Metascape analysis revealed enriched networks involving TC2R and other datasets, with a common 12-gene signature. The signature included PRC1, BIRC5, KIFC1, CDKN2A, MMP10, MMP3, TIMP1, ASPN, NPTX1, FOSL1, HMGA2, and FOXA2, and was associated with key pathways in *mitotic cell cycle*, *ECM organization*, *integrin1-syndecan/NABA core matrisome*, *cell junction organization*, *cell cycle regulation*, *senescence*, and *hormone regulation*. This signature could be largely validated as detectable or upregulated in human prostate cancer compared to normal tissues and correlated with reduced survival in a TCGA PRAD dataset. Further, the signature was significantly upregulated in PRAD iClusters 2 and 3[31], both of which indicate ETS protooncogene positive (ETS+) tumors; iCluster2 has homozygous deletions of PTEN and TP53 mutations, while iCluster3 has elevated PI3K/AKT, MAPK, and RTK pathways. Overall, these targets may be of special relevance for examining novel therapies for prostate cancer such as PI3K/AKT and other novel RTK inhibitors, gene therapies, and/or novel immunotherapies.

Our investigation into the immune landscape of TC2R tumors compared them with relevant genetically modified mouse models (GEMM), primarily focusing on p53 and/or Rb modifications from publicly available datasets. TC2R IT tumors exhibited increased NK cells in a non-activated state, varying levels of CD4 T memory cells, and increased M2 macrophages, contrasting with reduced M1 macrophages. These cell alterations could be driving more aggressive tumor growth in this model via immune evasion mechanisms. Similar immune profiles were observed in TC2R SC tumors, but with higher granulocytes, naïve B cells, fibroblasts, NK cells, and CD8-naïve cells compared to IT tumors. Both models showed fewer HSCs relative to normal prostate tissue, suggesting an immune suppressive environment. To validate these findings, we analyzed a human single-cell RNAseq dataset focused on bone-metastatic prostate cancer, confirming significant overlap with mouse datasets, particularly in CD4 Tmem cells, Treg cells, and M2 macrophages. The single-cell resolution enabled precise localization within tumors of dysfunctional T cell and monocytic lineages capable of contributing to immune suppression. Notably, T helper, T lineage progenitors, osteoblasts/fibroblasts, and pericytes were enriched within human tumors relative to surrounding bone marrow, while NK and NKT cells were more prevalent in involved bone marrow but excluded from tumors. Having less NK and NKT would contribute to an immune suppressive environment in the tumors. Strategies to enhance the infiltration of these innate response cells into tumors could mitigate rapid tumor growth. Various cytotoxic T and CD4 T mem cell populations were also identified within tumor tissues. The cytotoxic CTL1 (Kfoury et al., 2021) can enhance anti-tumor immunity in the presence of CD4 Tmem, to help provide long-term immune surveillance against tumor recurrence. The CTL2, a dysfunctional type (Kfoury et al., 2021), along with Treg, would suppress anti-tumor responses and promote immune evasion. The monocytic cell populations also were altered in the tumor fraction, mirroring results from the mouse datasets. This subset also contained diverse immune cell types such as inflammatory monocytes (TIMo), M1 and M2 macrophages, MDSC-like populations, myeloid DCs, B-naïve cells, neutrophils, progenitor cells, mast cells, and osteoclasts. Each cell type described here is likely to be influencing immune responses, tumor progression, and therapy outcomes. In combination, the findings from the TC2R model and their relevance to a human dataset suggest its potential for advancing immune-based interventions for prostate cancer patients.

Furthermore, we revisited the 12-gene signature identified in TC2R IT tumors in the single-cell RNAseq dataset. Several signature genes, including KIFC1, CDKN2A, PRC1, BIRC5, and ASPN, showed expression in relevant cell clusters such as progenitors/T cycling and osteoblasts/fibroblasts. In the monocytic subset, TIMP1 and other signature genes were detectable across multiple cell types, highlighting their potential roles in the tumor microenvironment. Expression patterns varied within cancer cell subsets, indicating heterogeneity in gene expression across different bone metastases. Our integrated analysis of networks, transcription factors, and enriched biological processes emphasized the similarities between the TC2R models and human prostate cancer. Of note, GEMM are relevant to prostate cancer due to their ability to mimic key mutations seen in human cases. PTEN, p53, and Rb mutations are common in primary prostate cancers (Abeshouse et al., 2015), affecting pathways critical for tumor development and progression. These mutations already indicate potential targets for therapeutic intervention, such as PI3K and Ras signaling inhibitors. Hras mutations are also observed in a subset of prostate cancers (Abeshouse et al., 2015), suggesting a role for Ras dysregulation in tumor pathogenesis. These models can serve as tools for testing new therapies aimed at specific genetic alterations found in prostate cancer patients, as shown recently for mutated p53 models which could model important immune and cell cycle features of tumors in younger (<50 years of age) prostate cancer patients (Mejía-Herná et al., 2022). These novel models are important in that they can be used to characterize emerging therapeutics expanding beyond the traditional anti-CTLA4 and anti-PD1 agents for prostate cancer patients.

The similarities with p53 null/mutant models in terms of pathways, transcription factors, and immune-related changes suggest that TC2R IT could offer insights into the intact immune cell repertoire, highlighting the role of immune responses in prostate cancer and potential for studying treatments, including immunotherapies. Despite p53 models being orthotopic (not bone), these similarities indicate unique cellular changes impacting pathways of proliferation and immunity. Finally, it is important to emphasize that TC2R is an intratibial implantation model, similar to the RM1 model, but with both osteoblastic and osteolytic lesions, whereas the RM1 model primarily exhibits osteolytic bone lesions. Nevertheless, bone implantation models remain valuable for testing therapeutics, offering advantages over GEMM in terms of cost, tumor take rate, and the ability of TC2R cells to seed and form human cancer-relevant bone lesions. This study presents the relevance of TC2R models, aligning with human prostate cancer pathways and highlighting key immune landscape features. We suggest that the TC2R IT model holds high utility in preclinical studies aimed at developing targeted therapies and personalized treatments. These efforts could later prove critical in improving prostate cancer patient survival and bone health.

5. Conclusion

In our study, we investigated gene expression changes in mouse models of prostate cancer, particularly the transition from less aggressive to more aggressive cells. We found that upregulated genes in TRAMP prostates were associated with cell cycle regulation and immune response, while downregulated genes in TC2 cells were related to various molecular functions and developmental processes. Comparisons between TRAMP, TC2, and TC2R highlighted distinct molecular signatures, including alterations in ECM organization, metabolism, and immune responses in TC2R cells. Subcutaneous and intratibial TC2R tumors exhibited unique gene expression profiles, indicating differences in their microenvironments and growth patterns. Furthermore, our analysis revealed significant similarities between TC2R models and human prostate cancer datasets in terms of pathways and immune landscape, suggesting the relevance of these mouse models. Overall, this research provides insights into the molecular mechanisms underlying prostate cancer using mouse models. The findings improve our understanding of prostate cancer biology and suggest that TRAMP models, with their similarities to other relevant mouse models and human prostate cancer cell lines and tumor samples, can serve as valuable tools for translating preclinical discoveries into clinical applications.

Conflict of interest

The authors declare that the research was conducted in the absence of any commercial or financial relationships that could be construed as a potential conflict of interest.

Funding

This project was funded by CA196947. We acknowledge support from the Basic Medical Sciences department at Purdue University. The authors gratefully acknowledge the support of the Collaborative Core for Cancer Bioinformatics (C^3B) from the Institute for Cancer Research, NIH grant P30 CA023168.

Data availability statement

Dataset 5 analyzed for this study is part of GSE248482 in NCBI GEO database. The remainder of the records already are in the NCBI GEO database, as indicated in Table S1 and Materials and Methods.

Declaration of interests

The authors declare that they have no known competing financial interests or personal relationships that could have appeared to influence the work reported in this paper.

CRediT authorship contribution statement

Marxa L. Figueiredo: Conceptualization, Data curation, Formal analysis, Funding acquisition, Investigation, Methodology, Project administration, Resources, Software, Supervision, Validation, Visualization, Writing – original draft, Writing – review & editing. **Sagar Utturkar:** Data curation, Methodology, Software, Writing – review & editing. **Shreya Kumar:** Methodology, Writing – review & editing. **Carlos Eduardo Fonseca-Alves:** Methodology, Software, Writing – original draft, Writing – review & editing.

Acknowledgments

The authors are grateful to Dr. Nadia Attalah (Purdue Cancer Center Computational Genomics, Bindley Bioscience Center) for coordinating and assisting with DEG determination and analysis.

Appendix A. Supplementary data

Supplementary data to this article can be found online at https://doi.org/10.1016/j.cellin.2024.100184.

References

Chen, W. B. R., Edmondson, E. F., & Waldmann, T. A. (2022). IL15 and anti-PD-1 augment the efficacy of agonistic intratumoral anti-CD40 in a mouse model with multiple TRAMP-C2 tumors. *Clinical Cancer Research, 28*, 2082–2093, 2010.1158/1078-0432.CCR-2021-0496.

Abeshouse, Adam, et al. (2015). The molecular taxonomy of primary prostate cancer. *Cell, 163*(4), 1011–1025. https://doi.org/10.1016/j.cell.2015.10.025

Chen, S., Zhou, Y., Chen, Y., & Gu, J. (2018). fastp: an ultra-fast all-in-one FASTQ preprocessor. *Bioinformatics, 34*, i884–i890. https://doi.org/10.1093/bioinformatics/bty560

DeCaprio, J. A., Ludlow, J. W., Figge, J., Shew, J. Y., Huang, C. M., Lee, W. H., Marsilio, E., Paucha, E., & Livingston, D. M. (1988). SV40 large tumor antigen forms a specific complex with the product of the retinoblastoma susceptibility gene. *Cell, 54*, 275–283. https://doi.org/10.1016/0092-8674(88)90559-4

Dobin, A., Davis, C. A., Schlesinger, F., Drenkow, J., Zaleski, C., Jha, S., Batut, P., Chaisson, M., & Gingeras, T. R. (2013). Star: Ultrafast universal RNA-seq aligner. *Bioinformatics, 29*, 15–21. https://doi.org/10.1093/bioinformatics/bts635

Dzojic, H. L. A., Tötterman, T. H., & Essand, M. (2006). Adenovirus-mediated CD40 ligand therapy induces tumor cell apoptosis and systemic immunity in the TRAMP-C2 mouse prostate cancer model. *The Prostate, 66*, 831–838, 810.1002/pros.20344.

Figueiredo Neto, M., Liu, S., Salameh, J. W., Yokota, H., & Figueiredo, M. L. (2020). Interleukin-27 gene delivery targeting IL-6rα-expressing cells as a stress response therapy. *International Journal of Molecular Sciences, 21*. https://doi.org/10.3390/ijms21031108

Foster, B. A., Gingrich, J. R., Kwon, E. D., Madias, C., & Greenberg, N. M. (1997). Characterization of prostatic epithelial cell lines derived from transgenic adenocarcinoma of the mouse prostate (TRAMP) model. *Cancer Research, 57*, 3325–3330.

Ge, S. X., Jung, D., & Yao, R. (2020). ShinyGO: A graphical gene-set enrichment tool for animals and plants. *Bioinformatics, 36*, 2628–2629. https://doi.org/10.1093/bioinformatics/btz931

Greenberg, N. M., DeMayo, F., Finegold, M. J., Medina, D., Tilley, W. D., Aspinall, J. O., Cunha, G. R., Donjacour, A. A., Matusik, R. J., & Rosen, J. M. (1995). Prostate cancer in a transgenic mouse. *Proceedings of the National Academy of Sciences of the United States of America, 92*, 3439–3443. https://doi.org/10.1073/pnas.92.8.3439

Hirz, T., Mei, S., Sarkar, H., Kfoury, Y., Wu, S., Verhoeven, B. M., Subtelny, A. O., Zlatev, D. V., Wszolek, M. W., Salari, K., Murray, E., et al. (2023). Dissecting the immune suppressive human prostate tumor microenvironment via integrated single-cell and spatial transcriptomic analyses. *Nature Communications, 14*, 663. https://doi.org/10.1038/s41467-023-36325-2

Ihle, C. L., Provera, M. D., Straign, D. M., Smith, E. E., Edgerton, S. M., Van Bokhoven, A., Lucia, M. S., & Owens, P. (2019). Distinct tumor microenvironments of lytic and blastic bone metastases in prostate cancer patients. *J Immunother Cancer, 7*, 293. https://doi.org/10.1186/s40425-019-0753-3

Kfoury, Y., Baryawno, N., Severe, N., Mei, S., Gustafsson, K., Hirz, T., Brouse, T., Scadden, E. W., Igolkina, A. A., Kokkaliaris, K., Choi, B. D., et al. (2021). Human prostate cancer bone metastases have an actionable immunosuppressive microenvironment. *Cancer Cell, 39*, 1464–1478.e1468. https://doi.org/10.1016/j.ccell.2021.09.005

Kido, L. A., de Almeida Lamas, C., Maróstica, M. R., & Cagnon, V. H. A. (2019). Transgenic adenocarcinoma of the mouse prostate (TRAMP) model: A good alternative to study PCa progression and chemoprevention approaches. *Life Sciences, 217*, 141–147. https://doi.org/10.1016/j.lfs.2018.12.002

Lane, D. P., & Crawford, L. V. (1979). T antigen is bound to a host protein in SV40-transformed cells. *Nature, 278*, 261–263. https://doi.org/10.1038/278261a0

Lardizabal, J. D. J., Delwar, Z., Rennie, P. S., & Jia, W. (2018). A TRAMP-derived orthotopic prostate syngeneic (TOPS) cancer model for investigating anti-tumor treatments. *The Prostate, 78*, 457–468, 410.1002/pros.23490. Epub 22018 Feb 23416.

Li, T., Fu, J., Zeng, Z., Cohen, D., Li, J., Chen, Q., Li, B., & Liu, X. S. (2020). TIMER2.0 for analysis of tumor-infiltrating immune cells. *Nucleic Acids Research, 48*, W509–W514. https://doi.org/10.1093/nar/gkaa407

Liao, Y., Smyth, G. K., & Shi, W. (2014). featureCounts: an efficient general purpose program for assigning sequence reads to genomic features. *Bioinformatics, 30*, 923–930. https://doi.org/10.1093/bioinformatics/btt656

Linzer, D. I., & Levine, A. J. (1979). Characterization of a 54K dalton cellular SV40 tumor antigen present in SV40-transformed cells and uninfected embryonal carcinoma cells. *Cell, 17*, 43–52. https://doi.org/10.1016/0092-8674(79)90293-9

Lu, Y., Starkey, N., Lei, W., Li, J., Cheng, J., Folk, W. R., & Lubahn, D. B. (2015). Inhibition of hedgehog-signaling driven genes in prostate cancer cells by sutherlandia frutescens extract. *PLoS One, 10*, Article e0145507. https://doi.org/10.1371/journal.pone.0145507

Mejía-Hernández, J. O., Keam, S. P., Saleh, R., Muntz, F., Fox, S. B., Byrne, D., Kogan, A., Pang, L., Huynh, J., Litchfield, C., Caramia, F., et al. (2022). Modelling aggressive prostate cancers of young men in immune-competent mice, driven by isogenic Trp 53 alterations and Pten loss. *Cell Death & Disease, 13*, 777. https://doi.org/10.1038/s41419-022-05211-y

Miao, Y. R., Zhang, Q., Lei, Q., Luo, M., Xie, G. Y., Wang, H., & Guo, A. Y. (2020). ImmuCellAI: A unique method for comprehensive T-cell subsets abundance prediction and its application in cancer immunotherapy. *Advanced Science, 7*, Article 1902880. https://doi.org/10.1002/advs.201902880

Robinson, M. D., McCarthy, D. J., & Smyth, G. K. (2010). edgeR: a Bioconductor package for differential expression analysis of digital gene expression data. *Bioinformatics, 26*, 139–140. https://doi.org/10.1093/bioinformatics/btp616

Shannon, P., Markiel, A., Ozier, O., Baliga, N. S., Wang, J. T., Ramage, D., Amin, N., Schwikowski, B., & Ideker, T. (2003). Cytoscape: A software environment for integrated models of biomolecular interaction networks. *Genome Research, 13*, 2498–2504. https://doi.org/10.1101/gr.1239303

Shen, R., Olshen, A. B., & Ladanyi, M. (2009). Integrative clustering of multiple genomic data types using a joint latent variable model with application to breast and lung cancer subtype analysis. *Bioinformatics, 25*, 2906–2912. https://doi.org/10.1093/bioinformatics/btp543

Tang, Z., Kang, B., Li, C., Chen, T., & Zhang, Z. (2019). GEPIA2: An enhanced web server for large-scale expression profiling and interactive analysis. *Nucleic Acids Research, 47*, W556–W560. https://doi.org/10.1093/nar/gkz430

Umbaugh, C. S., Diaz-Quiñones, A., Neto, M. F., Shearer, J. J., & Figueiredo, M. L. (2018). A dock derived compound against laminin receptor (37 LR) exhibits anti-cancer properties in a prostate cancer cell line model. *Oncotarget, 9*, 5958–5978. https://doi.org/10.18632/oncotarget.23236

Wu, R., Li, S., Sargsyan, D., Yin, R., Kuo, H. C., Peter, R., Wang, L., Hudlikar, R., Liu, X., & Kong, A. N. (2021). DNA methylome, transcriptome, and prostate cancer prevention by phenethyl isothiocyanate in TRAMP mice. *Molecular Carcinogenesis, 60*, 391–402. https://doi.org/10.1002/mc.23299

Yu, Z., Zou, H., Wang, H., Li, Q., & Yu, D. (2020). Identification of key gene signatures associated with bone metastasis in castration-resistant prostate cancer using Co-expression analysis. *Frontiers in Oncology, 10*, Article 571524. https://doi.org/10.3389/fonc.2020.571524

Zhou, Y., Zhou, B., Pache, L., Chang, M., Khodabakhshi, A. H., Tanaseichuk, O., Benner, C., & Chanda, S. K. (2019). Metascape provides a biologist-oriented resource for the analysis of systems-level datasets. *Nature Communications, 10*, 1523. https://doi.org/10.1038/s41467-019-09234-6

Zolochevska, O., Ellis, J., Parelkar, S., Chan-Seng, D., Emrick, T., Wei, J., Patrikeev, I., Motamedi, M., & Figueiredo, M. L. (2013). Interleukin-27 gene delivery for modifying malignant interactions between prostate tumor and bone. *Human Gene Therapy, 24*, 970–981. https://doi.org/10.1089/hum.2013.091